NJC

Accepted Manuscript

This is an *Accepted Manuscript*, which has been through the Royal Society of Chemistry peer review process and has been accepted for publication.

Accepted Manuscripts are published online shortly after acceptance, before technical editing, formatting and proof reading. Using this free service, authors can make their results available to the community, in citable form, before we publish the edited article. We will replace this *Accepted Manuscript* with the edited and formatted *Advance Article* as soon as it is available.

You can find more information about *Accepted Manuscripts* in the Information for Authors.

Please note that technical editing may introduce minor changes to the text and/or graphics, which may alter content. The journal's standard Terms & Conditions and the Ethical guidelines still apply. In no event shall the Royal Society of Chemistry be held responsible for any errors or omissions in this *Accepted Manuscript* or any consequences arising from the use of any information it contains.

ROYAL SOCIETY OF CHEMISTRY

www.rsc.org/njc

[1]Fabrication of Fe_3O_4@SiO_2@mSiO_2-HPG-COOH-Pd(0) Supported Catalyst and Its Performance in Catalyzing Suzuki Cross-Coupling Reaction

Wei Li,[a,b] Yi Tian,[a,b] Baoliang Zhang,[a,b] Lei Tian,[a,b] Xiangjie Li,[a,b] Hepeng Zhang,[a,b] Nisar Ali,[a,b] Qiuyu Zhang*,[a,b]

[a]Department of Applied Chemistry, College of Science, Northwestern Polytechnical University, Xi'an 710072, China.

[b]Key Laboratory of Space Physics and Chemistry, Ministry of Education, Northwestern Polytechnical University, P. O. Box 624, Xi'an 710072, China.

Abstract: In this paper, magnetic Fe_3O_4@SiO_2@mSiO_2 microspheres with core-shell structure were chosen as catalyst support, then the hyperbranched polyglycerol (HPG) was successfully grafted onto the exterior surface and mesopore wall of this material under the catalysis of isopropanol aluminum. Subsequently, the terminal hydroxyl groups of HPG were successfully transformed into carboxyl groups after the modification with succinic anhydride. Ultimately, palladium nanoparticles (Pd NPs) were successfully anchored onto the surface of aforementioned magnetic Fe_3O_4@SiO_2@mSiO_2 microspheres with carboxylic HPG in the form of high density and nanocrystallization by the complexation between Pd^{2+} ions and carboxyl groups and the following reduction, and a novel Fe_3O_4@SiO_2@mSiO_2-HPG-COOH-Pd(0) supported catalyst was successfully obtained. This novel supported Pd NPs catalyst is very conducive to the transference and exchanges of each component in the reaction system for the orderly mesoporous opening structure. Furthermore, the introduction of magnetism nucleus can provide a convenient magnetic separation. More

[1] Phone: +86-029-88431675, Fax: +86-029-88431675, E-mail: qyzhang@nwpu.edu.cn (Qiuyu Zhang).

importantly, the plenty of terminal carboxyl groups on the surface of magnetic Fe_3O_4@SiO_2@mSiO_2 microspheres can provide plenty of sufficient binding sites for Pd NPs, and the unique hyperbranched structure is very conducive to the capture of nano-sized palladium in the form of good dispersion and can effectively enhance the catalytic activity and stability. Research indicates that this novel suported Pd NPs catalyst not only possesses extremely high Pd NPs loading capacity but also shows remarkable catalytic activity to Suzuki cross-coupling reaction between aryl halides and phenylboronic acid. Simultaneously, the catalytic activity of this supported catalyst would not show evident loss after being used at least eight times.

Keywords: magnetic response, mesoporous silica, polyglycerol, palladium, Suzuki coupling reaction

1 Itroduction

In the past decades, because mesoporous silica retains many advantages such as high specific surface area and pore volume, tunable pore size, favorable biocompatibility, superior permeability, fast mass transfer and easy of surface modification, etc, it had been widely applied in separation [*1–4*], catalysis [*5–8*], sensor [*9–12*], biomedicine [*13–16*] and imprinting [*17–20*], etc. Kros et al.[*21*] prepared a folic acid-modified mesoporous silica nanoparticles, then this material was successfully applied in cellular and nuclear targeted drug delivery. Patel et al.[*22*] prepared the Co-B nanoparticle catalysts supported on mesoporous silica and study the effect of support pore structure on the catalytic properties in H_2 production by hydrolysis of ammonia borane. Biesuz et al.[*23*] synthesized a novel DFO-SAM on mesoporous silica for iron sensing by a new one-pot synthesis, and the kinetics of sorption reveals that the iron uptake is relatively fast, around 100 min at pH=2.5, from the sorption profile of iron(III), the estimated capacity of the product obtained under optimized conditions was higher than 0.3 $mmol \cdot g^{-1}$. Connor et al.[*24*] synthesized a class of mesoporous silica material (FDU-12) with different pore sizes and amine functionalization, then they determine its potential to differentially adsorb and separate dairy proteins. It was shown that the pore size of unfunctionalised FDU-12 is an important factor in the protein adsorption capacity. In this context, the application of mesoporous silica materials is throughout the various fields.

Mesoporous silica has indeed shown its own unique superiorty in its applications, but its recycle is

certainly a important issue to be resolved. Undoubtedly, it is one of the most effective means to fulfill the convenient separation of mesoporous silica by introducing magnetic nucleus into mesoporous silica microspheres, certainly, it has attracted many attentions of researchers [*25-29*]. Recently, it is a hot subject in the research field to use magnetic mesoporous microspheres as catalyst carriers. However, simple surface functionalization is very difficult to simultaneously achieve the nanocrystallization of noble metal catalyst and super high density loads. In addition, precious metals are particularly vulnerable during use, which would reduce the activity of catalyst to some extent and is obviously considered wasteful. Consequently, it is particularly essential to perform a specific surface modification on the surface of mesoporous microspheres to improve the load density, use stability and catalytic activity of supported catalyst. Zhao et al.[*30*] reported the fabrication of multifunctional microspheres which possess a core of nonporous silica-protected magnetite particles, transition layer of active gold nanoparticles, and an outer shell of ordered mesoporous silica with perpendicularly aligned pore channels. The unique nanostructure made the microsphere to be a novel stable and approachable catalyst system for various catalytic industry processes. Cravotto et al.[*31*] prepared a highly functionalized β-Cyclodextrin-Grafted Silica by the microwave irradiation. Bahnemann et al.[*32*] modified the mesoporous silica via the co-condensation of 2-(4-chlorosulfonylphenyl)ethyltrimethoxysilane and tetraethyl orthosilicate, then the TiO_2 particles were immobilized on the mesopore channels. Ha et al.[*25*] synthesized a core-shell magnetic mesoporous silica hybrid nanoparticles, then the boron-specificcis-diol was produced on this material surface by further modification with a glycidol reagent.

Based on our fundamental researches before, a good strategy to resolve aforementioned problems had been proposed, which is to modify the surface of magnetic mesoporous silica microspheres with hyperbranched structure. To our knowledge, it can introduce plenty of ligands to the material surface, which can effectively capture noble metal ions and stabilize the noble metal nanocatalyst for the special spatial conformation. Previously, the grafting of hyperbranched polyglycerol on the surface of magnetic Fe_3O_4@SiO_2 microspheres had been successively carried out by Xu, Neoh and Li et al.[*33-35*], and all the results are satisfactory. Unexpectedly, it is not satisfied to graft hyperbranched polyglycerol on the surface of magnetic mesoporous silica microspheres by the same method, which is mainly because the presence of a large number of mesoporous opening structure in the mesoporous silica coating reduces the network stability in the potassium methoxide system to some

extent. Therefore, the mesoporous silica coating would be easily etched by the highly alkaline potassium methoxide, and the complete core-shell structure grafted with hyperbranched polyglycerol can not be obtained. Through repeated experiments and tests, aluminium isopropoxide was chosen as the catalyst, ultimately, the hyperbranched polyglycerol was successfully grafted chemically on the surface of magnetic mesoporous silica microspheres but without significant influence to the morphology of mesoporous silica coating. On this basis, the terminal hydroxyl groups of hyperbranched polyglycerol were successfully transformed into carboxyl groups by the modification of succinic anhydride, which can provides a large number of binding sites for capturing Pd^{2+} ions. Because of the effective combination between orderly mesoporous opening structure and hyperbranched segment structure, this asprepared novel supported Pd NPs catalyst had displayed more superior performance compared with conventional supported catalyst, and this may make its due contribution to the effective reduction of use-cost.

2 Experimental

2.1 Reagents and Materials. Ferric chloride hexahydrate ($FeCl_3 \cdot 6H_2O$), sodium acetate (NaOAc), trisodium citrate, tetraethyl orthosilicate (TEOS), $NH_3 \cdot H_2O$ (28 wt%, A. R.), hexadecyltrimethylammonium bromide (CTAB), aluminium isopropoxide (98 wt%), anhydrous tetrahydrofuran (THF), anhydrous dioxane, glycidol (96 wt%), γ-aminopropyltriethoxysilane (APTES), anhydrous ethanol, $PdCl_2$, sodium borohydride ($NaBH_4$), and all of the chemical reagents were purchased from Sigma-Aldrich and were used without further treatment.

2.2 Modification of Fe_3O_4@SiO_2@mSiO_2 with Amino-Group. The magnetic mesoporous Fe_3O_4@SiO_2@mSiO_2 composite microspheres, which were prepared by optimizing our previous method [*36*], were functionalized by APTES to introduce amono-groups on the material surface. Primarily, 1.0 g of Fe_3O_4@SiO_2@mSiO_2 was uniformly dispersed in 80 mL of anhydrous ethanol with the aid of ultrasound. Then, 4 mL of APTES was dropwise added into aforementioned suspension, and the system was kept for 12 h under vigorous agitation at 45℃. After the reaction finished, the amino-functionalized composite microspheres were collected by applying an external magnet and washed 3~5 times with ethanol. Finally, the as-prepared sample was dried for 24 h via the vacuum freeze-drying technology, then the dried amino-functionalized magnetic mesoporous

Fe_3O_4@SiO_2@mSiO_2 composite microspheres were obtained. (The product was expressed as Fe_3O_4@SiO_2@mSiO_2-NH_2.)

2.3 Grafting of Hyperbranched Polyglycerol on Fe_3O_4@SiO_2@mSiO_2-NH_2. The grafting of hyperbranched polyglycerol on the surface of core-shell magnetic mesoporous Fe_3O_4@SiO_2@mSiO_2 composite microspheres was carried out by chemical grafting and polycondensation. Typically, aforementioned Fe_3O_4@SiO_2@mSiO_2-NH_2 were uniformly dispersed in 150 mL of anhydrous dioxane with the aid of ultrasound, then 0.5 g of isopropyl-aluminium was added into this suspension when the temperature was rose to 80℃. At the same time, the mixed system need to been protected under nitrogen atmosphere for 2 h to remove isopropanol generated in reaction. Subsequently, the dioxane was removed via the vacuum distillation at 40℃, and the magnetic mesoporous composite microspheres with a lot of active sites were successfully obtained. Then, the activated composite microspheres were redispersed into 150 mL of anhydrous dioxane under ultrasound. Subsequently, the temperature was adjusted to 80℃, and 20 mL of anhydrous dioxane containing 1 mL of glycidol was slowly added into the mixed system during 7 h. Then, the system was kept for 24 h at 80℃ under the protection of nitrigen atmosphere. After the reaction finished, the as-prepared sample was collected by applying an external magnet and quenched with ethanol. Then, the product was washed several times with ethanol and distilled water to remove the unreacted glycidol and its oligomer residue on the surface of magnetic mesoporous composite microspheres. Ultimately, the as-prepared product was dried for 24 h via the vacuum freeze-drying technology, then the hyperbranched product was successfully obtained. (Here, it was expressed as Fe_3O_4@SiO_2@mSiO_2-HPG.)

2.4 Carboxyl Functionalization of the Fe_3O_4@SiO_2@mSiO_2-HPG. Fe_3O_4@nSiO_2@mSiO_2-HPG was successfully modified with succinic anhydride according to the method in literature [*33*]. Typically, 1.0 g of Fe_3O_4@SiO_2@mSiO_2-HPG was uniformly dispersed into 150 mL of pyridine with the aid of ultrasound, then 0.6 g of succinic anhydride was added into aforementioned suspension, and this mixed system was stirred vigorously for 8 h under argon atmosphere in the dark. Subsequently, the product was collected by applying an external magnet and eluted several times with methanol. Finally, the product was washed several times with ethanol and distilled water and dried for 24 h via the vacuum freeze-drying technology. (Here, it was expressed as Fe_3O_4@SiO_2@mSiO_2-HPG-COOH.)

2.5 Preparaton of Fe_3O_4@SiO_2@mSiO_2-HPG-COOH-Pd(0) supported catalyst. Palladium nanoparticles were successfully anchored on the surface of Fe_3O_4@SiO_2@mSiO_2-HPG-COOH by the complexation between Pd^{2+} ions and carboxyl groups and the following reduction of Pd^{2+} ions. Primarily, 0.8 g of Fe_3O_4@SiO_2@mSiO_2-HPG-COOH and 70.0 mg of $PdCl_2$ were uniformly dispersed into 60 mL of anhydrous ethanol with the aid of ultrasound, then the mixed system was stirred for 24 h under the speed of 260 rpm at 45℃. After the reaction finished, the product was collected by applying an external magnet and washed 2-3 times with distilled water to remove dissociative Pd^{2+} ions. Subsequently, the product was redispersed into 60 mL of anhydrous ethanol, then 100 mg of $NaBH_4$ was added into this system, and this mixed system was stirred vigorously for 12 h at room temperature. After the reaction finished, the as-prepared product was collected by applying an external magnet and washed several times with distilled water and dried for 24 h via the vacuum freeze-drying technology. (Here, it was represented as Fe_3O_4@SiO_2@mSiO_2-HPG-COOH-Pd(0).)

2.6 Suzuki coupling reactions of aryl halides. The Suzuki cross-coupling reactions were carried out under the catalysis of Fe_3O_4@SiO_2@mSiO_2-HPG-COOH-Pd(0). The precursor solution was composed of 1.2 mmol of phenylboronic acid, 1.0 mmol of aryl halides (chlorobenzene, bromobenzene, iodobenzene, 4-chloroacetophenone, 4-chloronitrobenzene, 4-chlorotoluene, 3-chlorotoluene and 2-chlorotoluene), 0.2764 g of K_2CO_3 and 10 mL of isopropyl alcohol. Then, right amount of Fe_3O_4@SiO_2@mSiO_2-HPG-COOH-Pd(0) (0.075 mol% Pd) was added into the precursor solution, and the system with a cooling reflux device was vigorously stirred for 8, 10 and 12 h at 80℃, respectively. Finally, the reaction yields were obtained by high performance liquid chromatography (HPLC).

The yields of Suzuki coupling reactions were calculated by following formulas:

$$\mathrm{ee} = \frac{\mathrm{W}_p/\mathrm{M}_p}{\mathrm{W}_{ah}/\mathrm{M}_{ah}} \times 100\% \quad (1)$$

W_p is the mass of the produced biphenyl or its derivatives after the reaction, and W_{ah} is the mass of aryl halides before the reaction. M_p and M_{ah} is the corresponding relative molecular mass of biphenyl (or its derivatives) and aryl halides, respectively.

$$\mathrm{W}_p = \mathrm{C}_P \times \mathrm{V}_P \quad (2)$$

C_p is the mass concentration of the produced biphenyl or its derivatives after the reaction, and V_p is the volume of the coupling reaction system after the reaction.

$$\frac{\overline{W}_p}{\overline{W}_{pr}} = \frac{C_p \cdot V_s}{C_{pr} \cdot V_s} = \frac{C_p}{C_{pr}} = \frac{A_p}{A_{pr}} \quad (3)$$

C_{pr} is the known mass concentration in the reference standard solution, and V_s is the volume of testing solution. A_p and A_{pr} is the corresponding peak areas of biphenyl or its derivatives in the reaction solution and in the standard solution, respectively.

The following formula can be obtained by joining three equations of above:

$$ee = \frac{A_p C_{pr} V_p M_{ah}}{A_{pr} M_p W_{ah}} \quad (4)$$

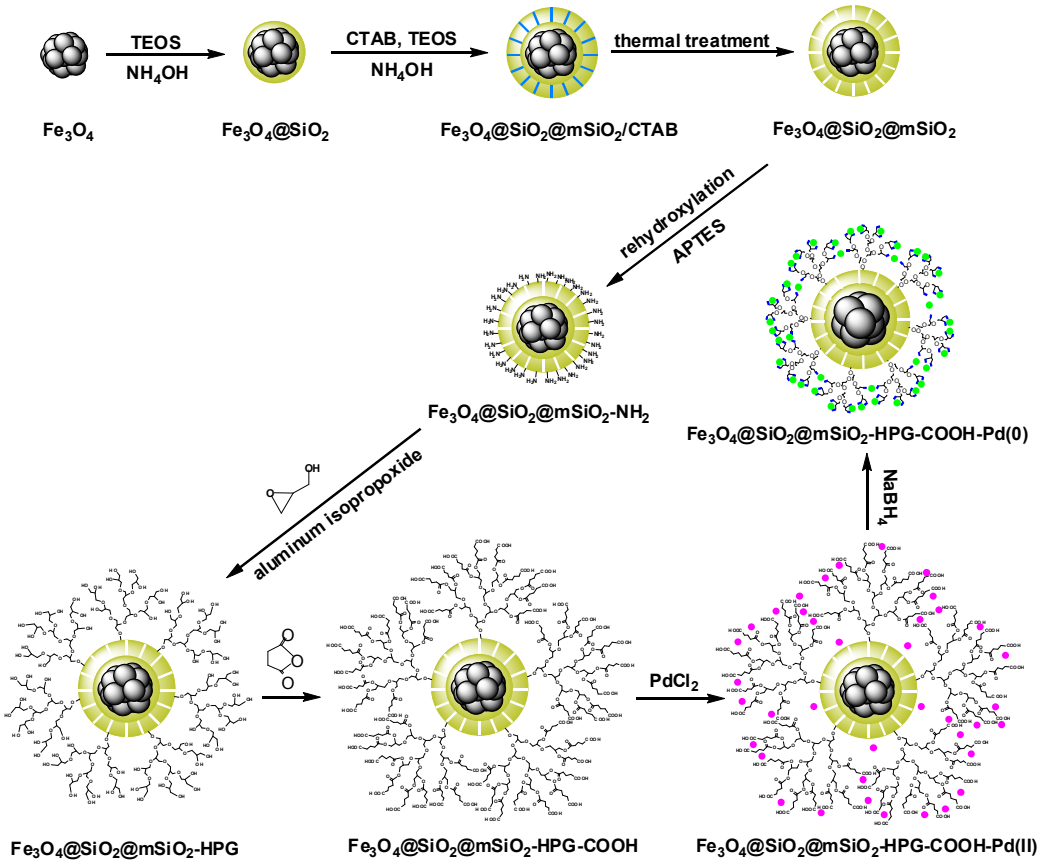

Scheme 1. Preparation process of the Fe_3O_4@SiO_2@mSiO_2-HPG-COOH-Pd(0).

2.7 Characterization. Fourier transform-infrared (FT-IR) spectra of samples were recorded on a Perkin-Elmer 580BIR spectrophotometer using the KBr pellet technique. X-ray powder diffraction (XRD) analysis was performed on a Bruker AXS D8-advance X-ray diffractometer with Cu Kα

radiation. N_2 adsorption/desorption isotherms were obtained on a TriStar II 20 apparatus. The pore size distribution was calculated from the adsorption branch of the N_2 adsorption/desorption isotherm and the Barret-Joyner-Halenda (BJH) method. The Brunauer-Emmett-Teller (BET) surface areas were determined by using the datas between 0.05 and 0.35 just before capillary condensation, and the pore volume was obtained by the t-plot method. The magnetic moment was recorded at 300 K on a JPMS-9H-EVERCOOL (QD) vibrating-sample magnetometer (VSM). Transmission electron microscopy (TEM), energy dispersive X-ray (EDS) spectra and transmission electron diffraction patterns were performed on a JEOL JEL2010 electron microscope at 200 kV. Scanning electron microscope (SEM) were performed on a FEISIRION 200 field-emission microscope. X-ray photoelectron spectroscopy (XPS) datas were collected to examine the chemical states of the multi-component photocatalyst with an Axis Ultra instrument (Kratos Analytical, Manchester, U.K.) under ultrahigh vacuum condition ($<10^{-6}$ Pa) and using a monochromatic Al Kα X-ray source (1486.6 eV). HPLC analysis was performed on a HITACHI L-2400. The ICP-AES was finished on an ICAP6300.

3 Results and discussion

3.1 Characterization of the Morphology of Materials

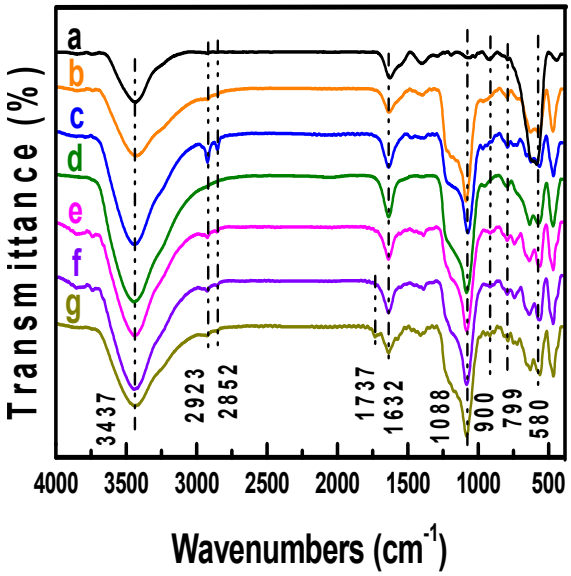

Fig.1 FTIR spectra of Fe_3O_4 (**a**), Fe_3O_4@SiO_2 (**b**), Fe_3O_4@SiO_2@mSiO_2/CTAB (**c**), Fe_3O_4@SiO_2@mSiO_2 (**d**), Fe_3O_4@SiO_2@mSiO_2-NH_2 (**e**), Fe_3O_4@SiO_2@mSiO_2-HPG (**f**) and Fe_3O_4@SiO_2@mSiO_2-HPG-COOH (**g**).

The preparation process of Fe_3O_4@SiO_2@mSiO_2-HPG-COOH-Pd(0) supported catalyst was

shown as scheme 1. At first, FTIR was applied to characterize the samples collected in each step (as shown in Fig.1**a-g**). It shows that all seven spectra have the adsorption peak corresponding to the characteristic absorption of Fe-O bond at 580 cm^{-1}. After being coated with silica, the characteristic absorption peaks corresponding to the antisymmetric and symmetric stretching vibration of Si-O-Si bond in oxygen-silica tetrahedron can be clearly observed at 1088 and 799 cm^{-1} (as Fig.1**b-g**). The characteristic absorption peaks at 2923 and 2852 cm^{-1} in Fig.1**c** can be attributed to the symmetric and antisymmetric stretching vibrations of ν_{C-H} in methyl and methylene of CTAB which exists in the outer shell. In comparison, the characteristic absorption peaks of ν_{C-H} disappeard after the high-temperature calcination, which indicates that the porogenic agent was removed completely after the high-temperature calcination (as Fig.1**d**). Subsequently, the magnetic mesoporous Fe_3O_4@SiO_2@$mSiO_2$ composite microspheres were functionalized with aminosilane, and a new absorption peak appeared at 900 cm^{-1} (Fig.1**e**), which must be attributed to the stretching vibration of γ_{N-H}. Besides, the adsorption peaks correspongding to the symmetric and antisymmetric stretching vibrations of ν_{C-H} in methylene can be observed again, which indicates that the amino-functionalization had been successfully achieved. Furthermore, HPG was grafted on the surface of the magnetic mesoporous Fe_3O_4@SiO_2@$mSiO_2$ composite microspheres by the ring-opening reaction and the following polycondensation, which can introduce plenty of hydroxyl groups to the surface of this composite microsphere. Compared with Fig.1**e**, the characteristic absorption peaks at 2923 and 2852 cm^{-1} had been increased (as Fig.1**f**), and the adsorption peak of ν_{O-H} at 3437 cm^{-1} had also increased to some extent, both of which indicates that the HPG had been successfully grafted on the surface of magnetic mesoporous Fe_3O_4@SiO_2@$mSiO_2$ composite microspheres. Finally, the terminal hydroxyl groups of HPG were transformed into carboxyl groups by succinic anhydride. As shown as Fig.1**g**, a new characteristic absorption peak corresponding to the stretching vibration of $\nu_{C=O}$ can be observed clearly at 1737 cm^{-1}, which indicates that the terminal hydroxyl groups had been successfully transformed into carboxyl groups, and the Fe_3O_4@SiO_2@$mSiO_2$-HPG-COOH had been successfully obtained.

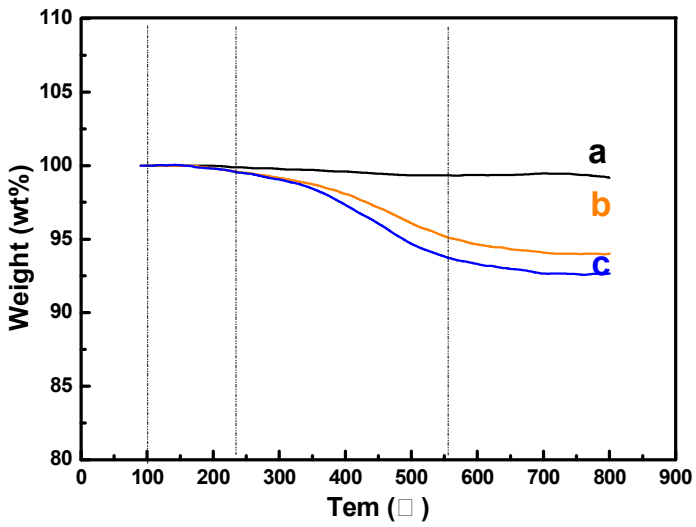

Fig.2 TG analysis of Fe_3O_4@SiO_2@mSiO_2 (**a**), Fe_3O_4@SiO_2@mSiO_2-HPG (**b**) and Fe_3O_4@SiO_2@mSiO_2-HPG-COOH (**c**).

To further confirm the successful implementation of the HPG grafting and carboxyl modification on the surface of magnetic mesoporous Fe_3O_4@SiO_2@mSiO_2 composite microspheres, thermogravimetric analysis (TG) was necessary to carry out. As shown as Fig.2, the trace amount of weight loss within the range of 100—200℃ is caused by the trace amount of water vapour adsorped by mesopore channels. Compared with Fig.2**a**, both of Fe_3O_4@SiO_2@mSiO_2-HPG and Fe_3O_4@SiO_2@mSiO_2-HPG-COOH has obvious weight loss within the range of 230—560℃, and the latter (~7.4%) is more than the former(~6.2%) (as Fig.2**b** and Fig.2**c**), which demonstrates that the HPG grafting and the carboxyl modification had been successfully achieved. Furthermore, both of carboxyl group content on the surface of Fe_3O_4@SiO_2-HPG-COOH and Fe_3O_4@SiO_2@mSiO_2-HPG-COOH was measured by the inverse titration method on the EasyPlus Titration of METTLER TOLEDO, and it is respectively 1.04 mmol/g and 2.13 mmol/g. Evidently, the latter is much more than the former. Which indicates that some small HPG segments were successfully introduced into the mesopore channels during the HPG grafting process, so the content of carboxyl groups on Fe_3O_4@SiO_2@mSiO_2-HPG-COOH is much larger than that of Fe_3O_4@SiO_2-HPG-COOH.

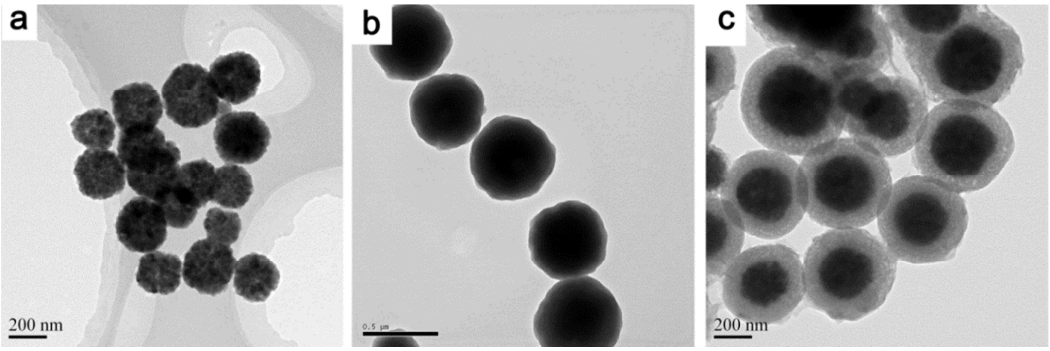

Fig.3 The TEM images of Fe_3O_4 (**a**), Fe_3O_4@SiO_2 (**b**) and Fe_3O_4@SiO_2@mSiO_2 (**c**).

Afterwards, the morphology of the microparticles obtained in every stage was characterized by TEM. As shown as Fig.3**a**, the magnetic Fe_3O_4 particles prepared by solvothermal method exhibit cauliflower-like morphology. The particle size is very uniform, which is about 200 nm. After being coated with a thin layer of dense silica, the core-shell structure can be clearly observed, and the thickness of the silica coating is about 60 nm (as Fig.3**b**). After a layer of mesoporous silica coating was coated on the outer surface of Fe_3O_4@SiO_2, the subsequent double-shell structure and mesopore structure appeared, and the thickness of the outer shell is about 80 nm (as Fig.3**c**).

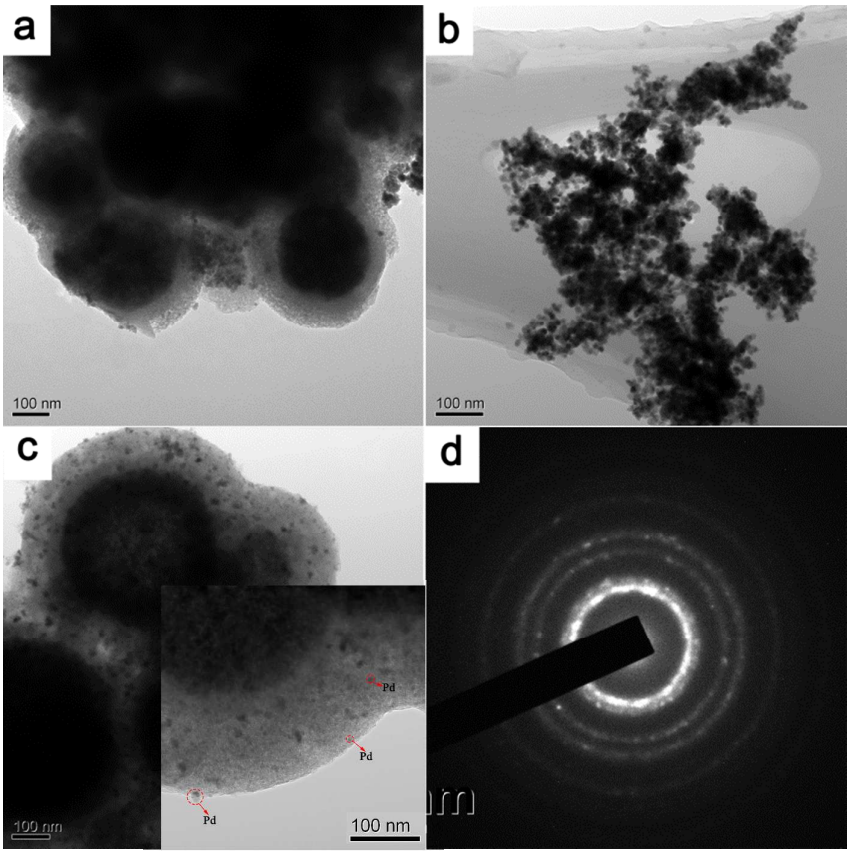

Fig.4 The TEM images of Fe_3O_4@SiO_2@mSiO_2-HPG-COOH-Pd(0) prepared in CH_3OK technique (**a** and **b**), in

isopropanol aluminum technique (**c**). (**d**) is the corresponding electron diffraction patterns of **c** and the insert is the magnified TEM image of **c**.

To the best of our knowledge, CH_3OK is the common catalyst for the HPG grafting on the surface of silica, so the HPG grafting on the surface of Fe_3O_4@SiO_2@$mSiO_2$ was also carried out by us, then this material was used to anchor Pd NPs catalyst. As shown as Fig.4**a** and Fig.4**b**, the double-shell structure was destroyed basically after this process, and the palladium aggregations were clearly observed near the supports. Which is because that the mesoporous silica coating had been etched for the strong alkaline of CH_3OK in the HPG grafting process, so that this material was unable to anchor the Pd NPs catalyst, and the etched material and palladium aggregations were obtained. Based on this problem, after a lot of tests, aluminium isopropylate was found to be a facile catalyst which can successfully catalyze the HPG grafting on the surface of mesoporous silica coating, so the Fe_3O_4@SiO_2@$mSiO_2$-HPG-COOH was also successfully obtained after the modification with succinic anhydride. Subsequently, Fe_3O_4@SiO_2@$mSiO_2$-HPG-COOH was applied to anchor the Pd NPs catalyst, and Fig.4**c** gives the TEM image of Fe_3O_4@SiO_2@$mSiO_2$-HPG-COOH-Pd(0) supported catalyst. Obviously, the Pd NPs with fcc structure (as Fig.4**d**), which partice size is about 5~10 nm, were successfully anchored on the surface of the Fe_3O_4@SiO_2@$mSiO_2$-HPG-COOH, and there was no any palladium aggregation to be observed. Which indicates that aluminium isopropylate is indeed a facile catalyst for the HPG grafting on the surface of mesoporous silica. Simultaneously, the unique three-dimensional conformation of the carboxylated HPG segments is very beneficial to the uniform dispersion of Pd NPs on the carriers, which can significantly increase the Pd NPs loading capacity, and the effective contact area between Pd NPs and reactants can also be increased for the uniform dispersion of Pd NPs. Therefore, it will be very conducive to the enhancement of the stability and catalytic activity of this novel supported Pd NPs catalyst. To further demonstrate the successful immobilization of Pd NPs, the EDX was necessary to carried out. Fig.5 shows that palladium indeed exists in the ultimate sample except iron, oxygen and silicon, which indicates the successful synthesis of the novel Fe_3O_4@SiO_2@$mSiO_2$-HPG-COOH-Pd(0) supported catalyst. In addition, the palladium loading capacity of this supported catalyst was examined by ICP-AES and was about 5.13 wt%, it was much larger than that of the previous Fe_3O_4@$nSiO_2$@$mSiO_2$-NH_2-Pd(0) supported catalyst [*25*], which demonstrates that the HPG segments indeed played an important role in anchoring Pd NPs catalyst on the surface of mesoporous silica.

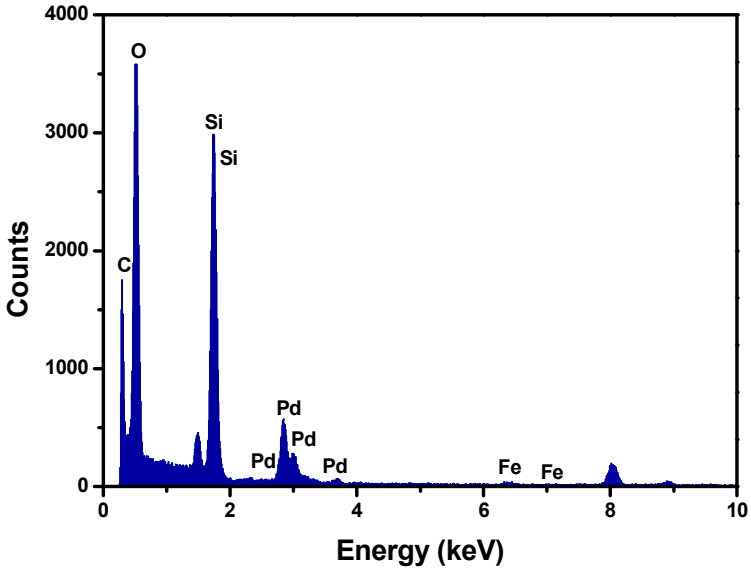

Fig.5 EDS spectrum of Fe_3O_4@SiO_2@mSiO_2-HPG-COOH-Pd(0) catalyst.

The XPS characterization provides further insight into the assessment of the surface composition of Fe_3O_4@SiO_2@mSiO_2-HPG-COOH-Pd(0) catalyst. The XPS spectrum in Fig.6**a** reveals that the surface of this supported catalyst was consisted with O, C, Pd and Si, and it indicates that the Pd catalyst should have been anchored on the surface of the core-shell magnetic mesoporous Fe_3O_4@SiO_2@mSiO_2 microspheres. Two peaks at 339.1 eV and 334.0 eV in Fig.6**b** were respectively attributed to $Pd^0 3d_{3/2}$ and $Bi^0 3d_{5/2}$, which indicates the existence of Pd(0) on the surface of the supports. It well demonstrates that the Pd NPs catalyst had been successfully anchored on the surface of the core-shell magnetic mesoporous Fe_3O_4@SiO_2@mSiO_2 microspheres.

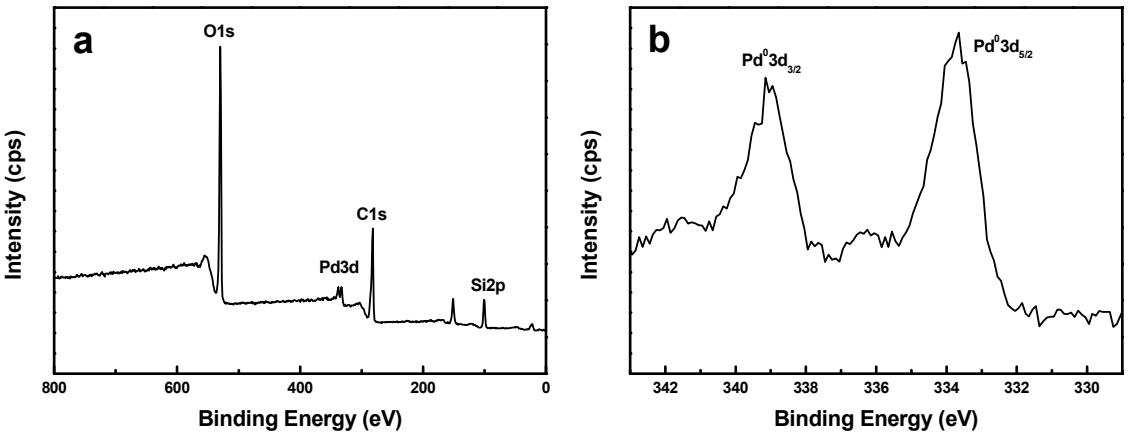

Fig.6 XPS spectra of Fe_3O_4@SiO_2@mSiO_2-HPG-COOH-Pd(0) catalyst: (**a**) survey and (**b**) Pd3d.

Furthermore, Fe_3O_4@SiO_2, Fe_3O_4@SiO_2@mSiO_2 and Fe_3O_4@SiO_2@mSiO_2-HPG-COOH-Pd(0) were characterized by N_2 adsorption/desorption, and the N_2 adsorption/desorption isotherms were

shown in Fig.7. The N_2 adsorption/desorption isotherms of core-shell magnetic Fe_3O_4@SiO_2 composite microspheres (Fig.7**a**) show a smooth curve, and the BET surface area is about 71.85 m^2/g. The adsorption of the material to nitrogen is not obvious, which further indicates that the silica shell of core-shell magnetic Fe_3O_4@SiO_2 composite microspheres is indeed dense and the porous structure is basically nonexistent. The N_2 adsorption/desorption isotherms of magnetic mesoporous Fe_3O_4@SiO_2@mSiO_2 composite microspheres is shown in Fig.7**b**, which displays a typical type Ⅳ isotherms with two inflection points in the relative pressure of 0.4 and 0.8, simultaneously, the hysteresis loops can be observed obviously. All of which indicates the existence of the mosopore structure. The BET surface area, BJH pore volume and pore size is ~203.98 m^2/g, ~0.2491 cm^3/g and 3—10 nm, respectively. The appropriate surface area and pore volume can provide a favorable space for anchoring Pd NPs. The N_2 adsorption/desorption isotherms of Fe_3O_4@SiO_2@mSiO_2-HPG-COOH-Pd(0) supported catalyst is shown in Fig.7**c**. Compared with the that of magnetic mesoporous Fe_3O_4@SiO_2@mSiO_2 composite microspheres, the N_2 adsorption capacity on this material reduced to some extent, and three inflection points in the relative pressure of 0.4, 0.8 and 0.9 can be observed clearly. Substantially, the main reason is that the magnetic mesoporous Fe_3O_4@SiO_2@mSiO_2 composite microspheres had changed more or less during the HPG grafting process, so some smaller Pd NPs might be introduced into the mesopore channels. Which ultimately leaded to the increase of some mesopores and the decrease of others. In addition, the measured BET surface area, BJH pore volume and pore size is respectively ~117.27 m^2/g, ~0.1809 cm^3/g and 3—13 nm, which is basically conformed to the aforementioned inference.

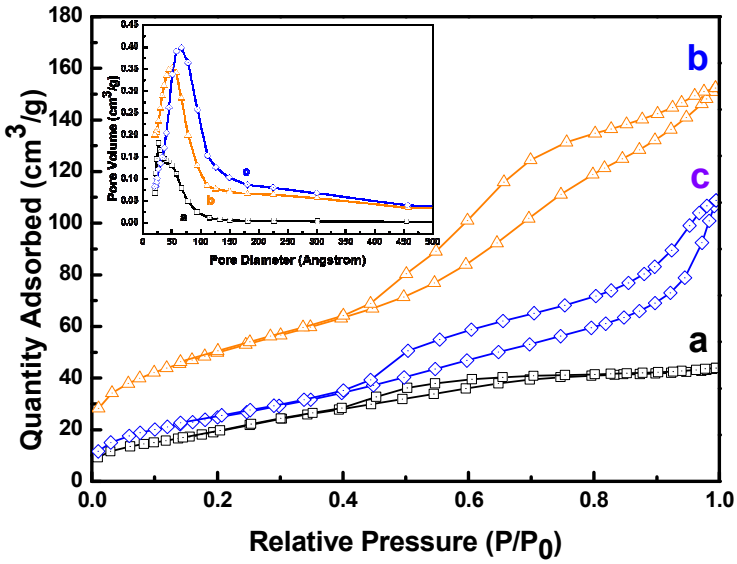

Fig.7 N_2 adsorption/desorption isotherms of Fe_3O_4@SiO_2 (**a**), Fe_3O_4@SiO_2@mSiO_2 (**b**) and Fe_3O_4@SiO_2@mSiO_2-HPG-COOH-Pd(0) (**c**), and the insert is the corresponding pore size distribution.

Afterwards, the crystalline structures of Fe_3O_4, Fe_3O_4@SiO_2@mSiO_2 and Fe_3O_4@SiO_2@mSiO_2-HPG-COOH-Pd(0) were determined by XRD. As displayed in Fig.8, six characteristic diffraction peaks (2θ = 30.2°, 35.6°, 43.3°, 53.8°, 57.3° and 63.0°) corresponding to (220), (311), (400), (422), (511) and (440) reflections of inverse spinel Fe_3O_4 can be observed clearly in all three curves. By comparing with Fig.8**a**, a broad peak around 2θ = 24° corresponding to the characteristic diffraction peak of amorphous silica can be observed (Fig.8**b** and Fig.8**c**). After anchoring Pd NPs catalyst, four characteristic diffraction peaks (2θ = 34°, 40°, 46° and 52°) corresponding to (311), (111), (200) and (422) reflections of palladium can be observed (Fig.8**c**), which also indicates the successful immobilization of Pd NPs with face-centered cubic structure. The amount of Pd NPs is very low relative to the carriers so that the diffraction peaks is very weak.

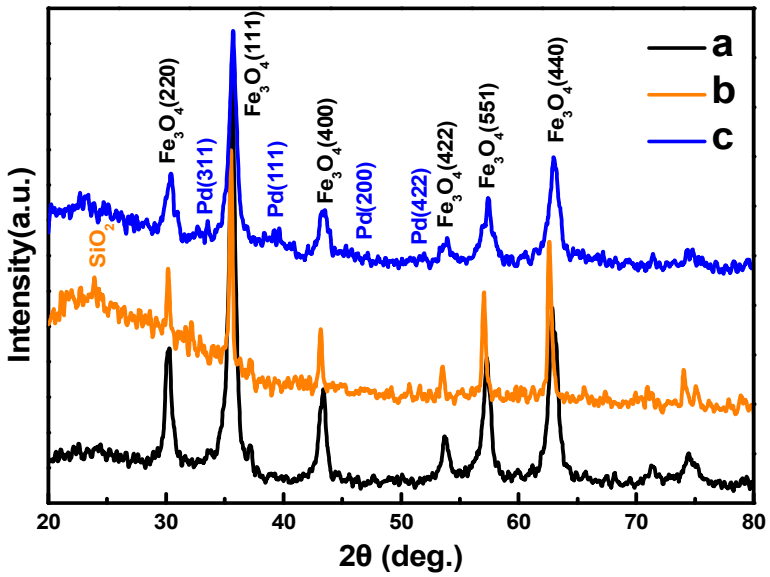

Fig.8 XRD pattern of Fe_3O_4 (**a**), Fe_3O_4@SiO_2@mSiO_2 (**b**) and Fe_3O_4@SiO_2@mSiO_2-HPG-COOH-Pd(0) (**c**).

To investigate the magnetic performance, Fe_3O_4, Fe_3O_4@SiO_2, Fe_3O_4@SiO_2@mSiO_2 and Fe_3O_4@SiO_2@mSiO_2-HPG-COOH-Pd(0) were characterized by VSM. Fig.9 shows that the magnetic saturation of aforementioned materials is about 80, 63, 35 and 30 emu/g, respectively, and the magnetization curves of four magnetic materials were confirmed a typical feature of superparamagnetism as no hysteresis is observed in low fields, which indicates that any remanence can not be observed after removing the external magnetic field. In summary, it indicates that all these magnetic materials can fulfill the simple separation requirment with the aid of external magnetic field. In addition, the inserted digital photos in Fig.9 show that this novel supported Pd NPs catalyst can be redispersed inot the original system after removing the external magnetic field, which can meet the application requirement well.

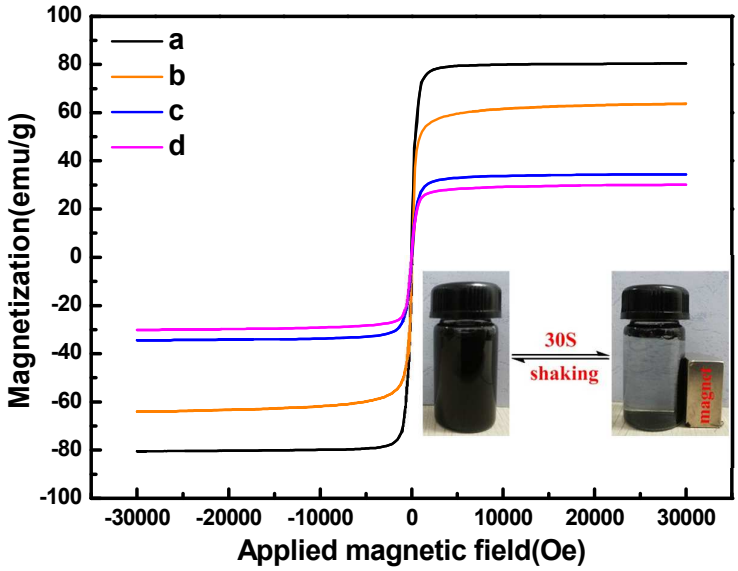

Fig.9 Magnetization curve of Fe_3O_4 (**a**), Fe_3O_4@SiO_2 (**b**), Fe_3O_4@SiO_2@mSiO_2 (**c**) and Fe_3O_4@SiO_2@mSiO_2-HPG-COOH-Pd(0) (**d**) measured at room temperature. And the insert is the corresponding magnetic seperation digital photos.

3.2 The Invesigation of the Catalytic Activity of the Novel Supported Catalyst

First of all, to investigate the influence of reaction time to the yields of Suzuki coupling reaction, 8 h, 10 h and 12 h were respectively chosen as the reaction time, and the corresponding reactions were finished at 80℃. Table 1 shows that the yield would increase to some extent as time goes on, then it would remain unchanged after reaching the maximum. For instance, the reaction of iodobenzene can be finished in 8 h, and the corresponding yield is about 99%. But the reactions of bromobenzene, 4-chloroacetophenone and 4-nitrochlorobenzene can be finished in 10 h, and the corresponding yield is about 91%, 96% and 92%, respectively. What is more, the reactions of chlorobenzene and its methyl substituded derivatives would require 12 h or even longer, which is mainly because that the electronegativity of the halogen substituent in aryl halide is weaker, the higher the reaction rate is, and the shorter the reaction time is. The electronegativity of Cl, Br and I from strong to weak is Cl＞Br＞I, so the corresponding reaction time of left would be longer than that of right.

Furthermore, the catalytic activity of this novel supported catalyst was also investigated by catalyzing a series of Suzuki coupling reactions for 10 h at three different temperatures. Table 1 shows that almost all the reaction yields reached the maximum at 80℃, and they were basically the same at 80℃ and 90℃, but it is relatively low at 70℃. The main reason is that both the breaking and formation of the chemical bond need enough energy, theoretically, when the reaction is carried

out at lower temperature, the energy supply is not enough to generate enough activated molecules to participate in the reaction, but when the reaction is carried out at higher temperature, it would generate more activated molecules for the sufficient energy supply in the system, so the reaction can be carried out effectively. It should be noted that excessive temperature may result in the formation of by-products, so we chose the appropriate temperature for this reaction, and here the reaction temperature was chosen as 80℃.

Table 1 The Suzuki coupling reactions of aryl halide and phenylboronic acid catalyzed by Fe_3O_4@SiO_2@mSiO_2-HPG-COOH-Pd(0) under different conditions.

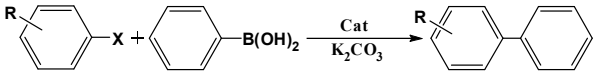

entry	Aryl halide	Product	Yield (%)[a]				
			8 h (80℃)	10 h (80℃)	12 h (80℃)	10 h (70℃)	10 h (90℃)
1		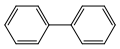	99	99	99	88	99
2		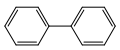	80	91	91	75	90
3		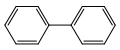	34	53	62	14	54
4	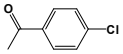	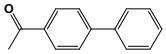	89	96	96	67	92
5	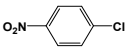	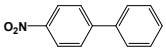	80	92	92	73	96
6	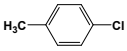	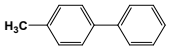	17	26	29	1	26
7	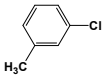	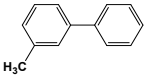	28	44	46	14	44
8		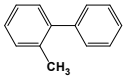	30	50	53	21	50

[a] HPLC yield based aryl halide.

Beyond that, substituent groups also have a big impact on the yield of reaction. By investigating the Suzuki coupling reaction of chlorobenzene and its derivations, it is not hard to find that the existence of electron-withdrawing in aryl halides is very conducive to the reaction and the existence of electron-donating group in aryl halides would lead to lower reaction yield. As shown in Table 1, the reaction yield of chlorobenzene is about 62%, and it is respectively about 96% and 92% to 4-chloroacetophenone and 4-nitrochlorobenzene, but it is only about 26% to 4-chlorotoluene. To the best of our knowledge, the difference of substitutional position also has an obvious impact on the reaction yield. By comparing the reaction yields of 4-chlorotoluene, 3-chlorotoluene and

2-chlorotoluene, it can be found that 2-chlorotoluene have the most high reaction yield (53%), 3-chlorotoluene is the second one (44%), and 4-chlorotoluene is the lowest one (26%). This is mainly because that methyl is ortho-para directing group, thus higher reaction yield would be obtained for methyl ortho-substituted chlorobenzene, which is basically matched with our previous study [*35*].

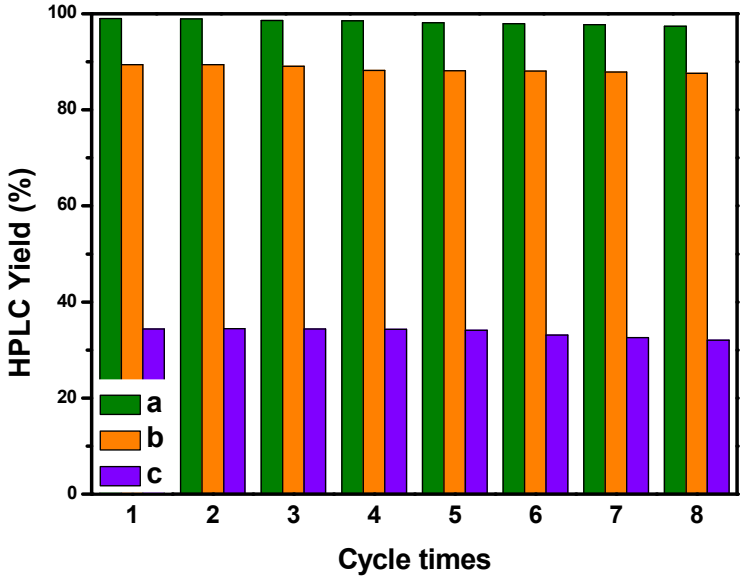

Fig.10 Investigation of the stability of Fe_3O_4@SiO_2@mSiO_2-HPG-COOH-Pd(0) in catalyzing Suzuki coupling reaction of iodobenzene (**a**), 4-chloroacetophenone (**b**) and chlorobenzene (**c**), respectively. The reaction time is 8 h.

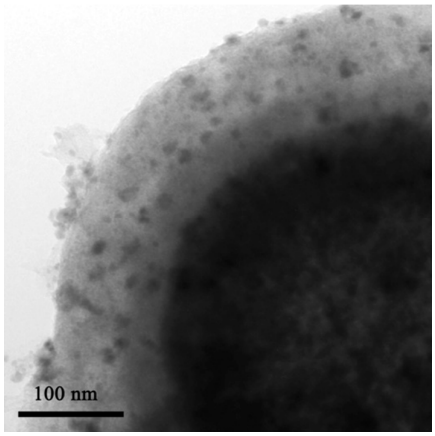

Fig.11 TEM image of the recovered Fe_3O_4@SiO_2@mSiO_2-HPG-COOH-Pd(0) supported catalyst after being used several times.

To further investigate whether the carboxylated HPG segments are conducive to the enhancement of the stability of this novel supported catalyst, it was regenerated and reused for several times.

Fig.10 displays the corresponding yields of the reused supported catalyst in the reaction time of 8 h, which indicates that the catalytic activity of this supported catalyst would not significantly decreased after being used eight times, and the yield can still respectively reach up to 97%, 88% and 32% for iodobenzene, 4-chloroacetophenone and chlorobenzene after being used eight times. Furthermore, the residual ratio to the original palladium content was 88.11% after the supported catalyst being used eight times by ICP-AES, and the TEM image of this novel supported catalyst after being used eight times had been also given. As shown as Fig.11, the palladium nanoparticles on the surface of the HPG grafted magnetic mesoporous Fe_3O_4@SiO_2@mSiO_2 microspheres still exhibited the ultrasmall nanoparticle morphology and good dispersion, and very small amounts of Pd aggragations can be observed. Which indicates that this novel Fe_3O_4@SiO_2@mSiO_2-HPG-COOH-Pd(0) supported catalyst shows very robust stability. All of which demonstrates that the HPG segments on the surface of Fe_3O_4@SiO_2@mSiO_2 can effectively stabilize Pd NPs through both the steric hindrance effect of HPG segments and complexation between Pd^{2+} ions and terminal carboxyl groups. Beyond that, the mesopore channels can also play an important role in stabilizing Pd NPs for some Pd NPs may enter the mesopore channel.

4 Conclusion

This paper mainly resolves the problem about the HPG grafting on the surface of mesoporous silica coating by choosing isopropanol aluminum as a facile catalyst, then the terminal hydroxyl groups of HPG were successfully transformed into carboxyl groups after the modification with succinic anhydride. Subsequently, Pd NPs were successfully anchored on the surface of aforementioned material through the complexation between Pd^{2+} ions and carboxyl groups and the following reduction, thus Fe_3O_4@SiO_2@mSiO_2-HPG-COOH-Pd (0) supported catalyst was successfully obtained. This novel supported Pd NPs catalyst is very conducive to the transference and exchanges of each component in the reaction system for the orderly mesoporous opening structure. Furthermore, the introduction of magnetism nucleus can provide a convenient magnetic separation. More importantly, the plenty of terminal carboxyl groups on the surface of magnetic Fe_3O_4@SiO_2@mSiO_2 microspheres can provide plenty of sufficient binding sites for Pd NPs, and the unique hyperbranched structure is very conducive to the capture of nano-sized palladium in the form of good dispersion and

can effectively enhance the catalytic activity and stability. Research indicates that this novel suported Pd NPs catalyst not only possesses extremely high Pd NPs loading capacity but also shows remarkable catalytic activity to Suzuki cross-coupling reaction between aryl halides and phenylboronic acid. Simultaneously, the catalytic activity of this supported catalyst would not show evident loss after being used at least eight times.

Acknowledgment

The authors are grateful for the financial support provided by the National Natural Science Foundation of China (No. 51173146 and NO. 21201140), basic research fund of Northwestern polytechnical university (3102014JCQ01094, 3102014ZD).

References

[1] H. Qin, Z. Hu, F. Wang, Y. Zhang, L. Zhao, G. Xu, R. Wu, H. Zou. Facile preparation of ordered mesoporous silica-carbon composite nanoparticles for glycan enrichment. *Chem. Commun*. 49 (2013) 5162–5164.

[2] D.-W. Lee, M.-H. Jin, C.-B. Lee, D. Oh, S.-K. Ryi, J.-S. Park, J.-S. Bae, Y.-J. Lee, S.-J. Park, Y.-C. Choi. Facile synthesis of mesoporous silica and titania supraparticles by a meniscus templating route on a superhydrophobic surface and their application to adsorbents. *Nanoscale* 6 (2014) 3483–3487.

[3] W. Yang, P. Ding, L. Zhou, J. Yu, X. Chen, F. Jiao. Preparation of diamine modified mesoporous silica on multi-walled carbon nanotubes for the adsorption of heavy metals in aqueous solution. *Appl. Surf. Sci.* 282 (2013) 38–45.

[4] X. Wan, S. Yao, H. Liu, Y. Yao. Selective fluorescence sensing of Hg^{2+} and Zn^{2+} ions through dual independent channels based on the site-specific functionalization of mesoporous silica nanoparticles. *J. Mater. Chem. A* 1 (2013) 10505–10512.

[5] H. Li, M. Yang, X. Zhang, L. Yan, J. Li and Y. Qi. Mesoporous silica-supported copper-catalysts for homocoupling reaction of terminal alkynes at room-temperature. *New J. Chem*. 37 (2013) 1343–1349.

[6] J. Long, G. Liu, T. Cheng, H. Yao, Q. Qian, J. Zhuang, F. Gao, H. Li. Immobilization of rhodium-based transfer hydrogenation catalysts on mesoporous silica materials. *J. Catal*. 298 (2013) 41–50.

[7] L. Shang, T. Bian, B. Zhang, D. Zhang, L.-Z. Wu, C.-H. Tung, Y. Yin, T. Zhang. Graphene-Supported Ultrafine Metal Nanoparticles Encapsulated by Mesoporous Silica: Robust Catalysts for Oxidation and Reduction Reactions. *Angew. Chem*. 126 (2014) 254–258.

[8] Fang Zhang, Mingzhen Chen, Xiaotao Wu, Wei Wang and Hexing Li. Highly active, durable and recyclable ordered mesoporous magnetic organometallic catalysts for promoting organic reactions in water. *J. Mater. Chem. A* 2 (2014) 484–491.

[9] S. K. Maji, S. Sreejith, A. K. Mandal, X. Ma, Y. Zhao. Immobilizing Gold Nanoparticles in Mesoporous Silica Covered Reduced Graphene Oxide: A Hybrid Material for Cancer Cell Detection through Hydrogen Peroxide Sensing. *ACS Appl. Mater. Interfaces* 6 (2014) 13648−13656.

[10] H. Cao, X. Hu, C. Hu, Y. Zhang, N. Jia. A novel solid-state electrochemiluminescence sensor for melamine with $Ru(bpy)_3^{2+}$/mesoporous silica nanospheres/Nafion composite modified electrode. *Biosens. Bioelectron.* 41 (2013) 911–915.

[11] G. Alberti, G. Emma, R. Colleoni, M. Pesavento, V. M. Nurchi, R. Biesuz. Novel DFO-functionalized mesoporous silica for iron sensing. Part 2. Experimental detection of free iron concentration (pFe) in urine samples. *Analyst* 139 (2014) 3940–3948.

[12] C.-J. Tsou, C.-Y. Chu, Y. Hung, C.-Y. Mou. A broad rangefluorescent pH sensor based on hollow mesoporous silica nanoparticles, utilising the surface curvature effect. *J. Mater. Chem. B* 1 (2013) 5557–5563.

[13] J. Liu, W. Bu, L. Pan, J. Shi. NIR-Triggered Anticancer Drug Delivery by Upconverting Nanoparticles with Integrated Azobenzene-Modified Mesoporous Silica. *Angew. Chem. Int. Ed*. 52 (2013) 4375–4379.

[14] H. Meng, W. X. Mai, H. Zhang, M. Xue, T. Xia, S. Lin, X. Wang, Y. Zhao, Z. Ji, J. T. Zink, A. E. Nel. Codelivery of an Optimal Drug/siRNA Combination Using Mesoporous Silica Nanoparticles To Overcome Drug Resistance in Breast Cancerin Vitro and in Vivo. *ACS Nano* 7 (2013) 994–1005.

[15] L. Bergman, P. Kankaanpää, S. Tiitta, A. Duchanoy, L. Li, J. Heino, M. Lindén. Intracellular Degradation of Multilabeled Poly(Ethylene imine)-Mesoporous Silica-Silica Nanoparticles: Implications for Drug Release. *Mol. Pharmaceutics* 10 (2013) 1795−1803.

[16] Y.-P. Chen, C.-T. Chen, Y. Hung, C.-M. Chou, T.-P. Liu, M.-R. Liang, C.-T. Chen, C.-Y. Mou. A New Strategy for Intracellular Delivery of Enzyme Using Mesoporous Silica Nanoparticles: Superoxide Dismutase. *J. Am. Chem. Soc*. 135 (2013) 1516−1523.

[17] C. Kang, W. Li, L. Tan, H. Li, C. Wei, Y. Tang. Highly ordered metal ion imprinted mesoporous silica particles exhibiting specific recognition and fast adsorption kinetics. *J. Mater. Chem. A* 1 (2013) 7147–7153.

[18] P. Kadhirvel, M. Azenha, A. F. Silva, B. Sellergren. Chromatographycally efficient microspherical composites of molecularly imprinted xerogels deposited inside mesoporous silica. *J. Chromatogr. A* 1355 (2014) 158–163.

[19] M. Meng, X. Meng, Y. Liu, Z. Liu, J. Hand, Y. Wanga, M. Luo, R. Chen, L. Nia, Y. Yan. An ion-imprinted functionalized SBA-15 adsorbent synthesized by surface imprinting technique via reversible addition-fragmentation chain transfer polymerization for selective removal of Ce(III) from aqueous solution. *J. Hazard. Mater*. 278 (2014) 134–143.

[20] F. Aboufazeli, H. R. L. Z. Zhad, O. Sadeghi, M. Karimi, E. Najafi. Novel ion imprinted polymer magnetic mesoporous silica nano-particles for selective separation and determination of lead ions in food samples. *Food Chem.* 141 (2013) 3459–3465.

[21] F. Porta, G. E. M. Lamers, J. Morrhayim, A. Chatzopoulou, M. Schaaf, H. D. Dulk, C. Backendorf, J. I. Zink, A. Kros. Folic Acid-Modified Mesoporous Silica Nanoparticles for Cellular and Nuclear Targeted Drug Delivery. *Adv. Healthcare Mater*. 2 (2013) 281–286.

[22] N. Patel, R. Fernandes, S. Gupta, R. Edla, D. C. Kothari, A. Miotello. Co-B catalyst supported over mesoporous silica for hydrogen production by catalytic hydrolysis of Ammonia Borane: A study on influence of pore structure. *Appl. Catal. B-Environ.* 140–*141 (*2013) 125–132.

[23] R. Biesuz, G. Emma, C. Milanese, G. Dacarro, A. Taglietti, V. M. Nurchi, G. Alberti. Novel DFO-SAM on mesoporous silica for iron sensing. Part I. Synthesis optimization and characterization of the material. *Analyst* 139 (2014) 3932–3939.

[24] M. N. Sarvi, T. B. Bee, C. K. Gooi, B. W. Woonton, M. L. Gee, A. J. O'Connor. Development of functionalized mesoporous silica for adsorption and separation of dairy proteins. *Chem. Eng. J.* 235 (2014) 244–251.

[25] M. S. Moorthy, D.-J. Seo, H.-J. Song, S. S. Park, C.-S. Ha. Magnetic mesoporous silica hybrid nanoparticles for highly selective boron adsorption. *J. Mater. Chem. A* 1 (2013) 12485–12496.

[26] J. Yang, F. Zhang, W. Li, D. Gu, D. Shen, J. Fan, W.-X. Zhang, D. Zhao. Large pore mesostructured cellular silica foam coated magnetic oxide composites with multilamellar vesicle shells for adsorption. *Chem. Commun*. 50 (2014) 713–715.

[27] J. Lee, S. Y. Lee, S. H. Park, H. S. Lee, J. H. Lee, B.-Y. Jeong, S.-E. Park, J. H. Chang. High throughput detection and selective enrichment of histidine-tagged enzymes with Ni-doped magnetic mesoporous silica. *J. Mater. Chem. B* 1 (2013) 610–616.

[28] X.-S. Li, Y.-N. Pan, Y. Zhao, B.-F. Yuan, L. Guob, Y.-Q. Feng. Preparation of titanium-grafted magnetic mesoporous silica for the enrichment of endogenous serum phosphopeptides. *J. Chromatogr. A* 1315 (2013) 61–69.

[29] D. Huang, Y. Sha, S. Zheng, B. Liu, C. Deng. Preparation of phenyl group-functionalized magnetic mesoporous silica microspheres for fast extraction and analysis of acetaldehyde in mainstream cigarette smoke by gas chromatography-mass spectrometry. *Talanta* 115 (2013) 427–434.

[30] Y. Deng, Y. Cai, Z. Sun, J. Liu, C. Liu, J. Wei, W. Li, C. Liu, Y. Wang, and D. Zhao. Multifunctional Mesoporous Composite Microspheres with Well-Designed Nanostructure: A Highly Integrated Catalyst System. *J. Am. Chem. Soc*. 132 (2010) 8466–8473.

[31] K. Martina, F. Baricco, G. Berlier, M. Caporaso, G. Cravotto. Efficient Green Protocols for Preparation of Highly Functionalized β-Cyclodextrin-Grafted Silica. Cravotto. *ACS Sustainable Chem. Eng*. 2 (2014) 2595–2603.

[32] A. Hakki, R. Dillert, D. W. Bahnemann. Arenesulfonic Acid-Functionalized Mesoporous Silica Decorated with Titania: A Heterogeneous Catalyst for the One-Pot Photocatalytic Synthesis of Quinolines from Nitroaromatic Compounds and Alcohols. *ACS Catal*. 3 (2013) 565−572.

[33] L. Zhou, C. Gao, W. Xu. Robust Fe_3O_4/SiO_2-Pt/Au/Pd Magnetic Nanocatalysts with Multifunctional Hyperbranched Polyglycerol Amplifiers. *Langmuir* 26 (2010) 11217–11225.

[34] L. Wang, K. G. Neoh, E.-T. Kang, B. Shuter. Multifunctional polyglycerol-grafted Fe_3O_4@SiO_2 nanoparticles for targeting ovarian cancer cells. *Biomaterials* 32 (2011) 2166–2173.

[35] Q. Du, W. Zhang, H. Ma, J. Zheng, B. Zhou, Y. Li. Immobilized palladium on surface-modified Fe_3O_4/SiO_2 nanoparticles: as a magnetically separable and stable recyclable high-performance catalyst for Suzuki and Heck cross-coupling reactions. *Tetrahedron* 68 (2012) 3577–3584.

[36] W. Li, B. Zhang, X. Li, H. Zhang. Q. Zhang. Preparation and characterization of novel immobilized Fe_3O_4@SiO_2@mSiO_2-Pd(0) catalyst with large pore-size mesoporous for Suzuki coupling reaction. *Appl. Catal. A-Gen*. 459 (2013) 65–72.